

## First tests of a reconfigurable depleted MAPS sensor for digital electromagnetic calorimetry

Allport, P. P.; Bosley, R.; Dopke, J.; Flynn, S.; Gonella, L.; Kopsalis, I.; Nikolopoulos, K.; Phillips, P. W.; Price, T.; Scott, A.; Sedgwick, I.; Villani, E. G.; Warren, M.; Watson, N.; Wilson, F.; Winter, A.; Worm, S.; Zhang, Z.

DOI:

[10.1016/j.nima.2019.162654](https://doi.org/10.1016/j.nima.2019.162654)

License:

Creative Commons: Attribution-NonCommercial-NoDerivs (CC BY-NC-ND)

*Document Version*

Peer reviewed version

*Citation for published version (Harvard):*

Allport, PP, Bosley, R, Dopke, J, Flynn, S, Gonella, L, Kopsalis, I, Nikolopoulos, K, Phillips, PW, Price, T, Scott, A, Sedgwick, I, Villani, EG, Warren, M, Watson, N, Wilson, F, Winter, A, Worm, S & Zhang, Z 2019, 'First tests of a reconfigurable depleted MAPS sensor for digital electromagnetic calorimetry', *Nuclear Instruments and Methods in Physics Research, Section A: Accelerators, Spectrometers, Detectors and Associated Equipment*. <https://doi.org/10.1016/j.nima.2019.162654>

[Link to publication on Research at Birmingham portal](#)

### General rights

Unless a licence is specified above, all rights (including copyright and moral rights) in this document are retained by the authors and/or the copyright holders. The express permission of the copyright holder must be obtained for any use of this material other than for purposes permitted by law.

- Users may freely distribute the URL that is used to identify this publication.
- Users may download and/or print one copy of the publication from the University of Birmingham research portal for the purpose of private study or non-commercial research.
- User may use extracts from the document in line with the concept of 'fair dealing' under the Copyright, Designs and Patents Act 1988 (?)
- Users may not further distribute the material nor use it for the purposes of commercial gain.

Where a licence is displayed above, please note the terms and conditions of the licence govern your use of this document.

When citing, please reference the published version.

### Take down policy

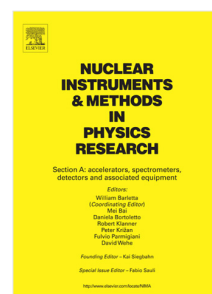
While the University of Birmingham exercises care and attention in making items available there are rare occasions when an item has been uploaded in error or has been deemed to be commercially or otherwise sensitive.

If you believe that this is the case for this document, please contact [UBIRA@lists.bham.ac.uk](mailto:UBIRA@lists.bham.ac.uk) providing details and we will remove access to the work immediately and investigate.

## Journal Pre-proof

First tests of a reconfigurable depleted MAPS sensor for digital electromagnetic calorimetry

P.P. Allport, R. Bosley, J. Dopke, S. Flynn, L. Gonella, I. Kopsalis, K. Nikolopoulos, P.W. Phillips, T. Price, A. Scott, I. Sedgwick, E.G. Villani, M. Warren, N. Watson, F. Wilson, A. Winter, S. Worm, Z. Zhang



PII: S0168-9002(19)31141-6  
DOI: <https://doi.org/10.1016/j.nima.2019.162654>  
Reference: NIMA 162654

To appear in: *Nuclear Inst. and Methods in Physics Research, A*

Received date : 30 March 2019  
Revised date : 27 August 2019  
Accepted date : 30 August 2019

Please cite this article as: P.P. Allport, R. Bosley, J. Dopke et al., First tests of a reconfigurable depleted MAPS sensor for digital electromagnetic calorimetry, *Nuclear Inst. and Methods in Physics Research, A* (2019), doi: <https://doi.org/10.1016/j.nima.2019.162654>.

This is a PDF file of an article that has undergone enhancements after acceptance, such as the addition of a cover page and metadata, and formatting for readability, but it is not yet the definitive version of record. This version will undergo additional copyediting, typesetting and review before it is published in its final form, but we are providing this version to give early visibility of the article. Please note that, during the production process, errors may be discovered which could affect the content, and all legal disclaimers that apply to the journal pertain.

© 2019 Published by Elsevier B.V.

## First tests of a reconfigurable depleted MAPS sensor for Digital Electromagnetic Calorimetry

P.P. Allport<sup>a</sup>, R. Bosley<sup>a</sup>, J. Dopke<sup>b</sup>, S. Flynn<sup>a</sup>, L. Gonella<sup>a</sup>, I. Kopsalis<sup>a,\*</sup>,  
K. Nikolopoulos<sup>a</sup>, P.W. Phillips<sup>b</sup>, T. Price<sup>a</sup>, A. Scott<sup>b</sup>, I. Sedgwick<sup>b</sup>,  
E.G. Villani<sup>a</sup>, M. Warren<sup>c</sup>, N. Watson<sup>a</sup>, F. Wilson<sup>b</sup>, A. Winter<sup>a</sup>, S. Worm<sup>a</sup>,  
Z. Zhang<sup>b</sup>

<sup>a</sup>*School of Physics and Astronomy, University of Birmingham, Edgbaston, B15 2TT, Birmingham, United Kingdom*

<sup>b</sup>*STFC Rutherford Appleton Laboratory, Harwell Campus, OX11 0QX, Didcot, United Kingdom*

<sup>c</sup>*Department of Physics and Astronomy, University College London, Gower Street, WC1E 6BT, London, United Kingdom*

---

### Abstract

Digital Electromagnetic CALorimetry relies on a highly granular detector where the cell size is sufficiently small so that only a single particle in a shower enters each cell within a single readout cycle. The DECAL sensor, a depleted monolithic active pixel sensor (DMAPS), has been proposed as a possible technology for future digital calorimeters. A DECAL sensor prototype has been designed and fabricated in the TowerJazz 180 nm CMOS imaging process, using a high resistivity 18  $\mu\text{m}$  epitaxial Si layer. The prototype has a pixel matrix of  $64 \times 64$  pixels with a pitch of  $55 \times 55 \mu\text{m}$ , and is read out using fast logic at 40 MHz. It can be configured to function as either a strip sensor, for particle tracking, or a pad sensor, counting the number of pixels above threshold for digital calorimetry. Preliminary results of chip characterisation, including digital summing logic, analogue pixel performance and threshold scans under laser illumination are presented.

**Keywords:** Digital Calorimetry, Depleted MAPS, Reconfigurable, Analogue Pixel, Pixel Configuration Logic

---

---

\*Corresponding author. Email address: Ioannis.Kopsalis@stfc.ac.uk

## 1. Introduction

Electromagnetic calorimeters (ECALs) rely on the principle that the number of charged particles travelling each layer is on average proportional to the incident particle energy. However, there are fluctuations around this average due to the stochastic nature of the shower development. The charged particles lose energy in traversing the sensitive layers of the ECAL, and the energy loss per particle also has fluctuations. These are due to the Landau distribution of the deposited energy but also due to variations in their velocity and path length through the material [1]. So far, the energy resolution of an analogue

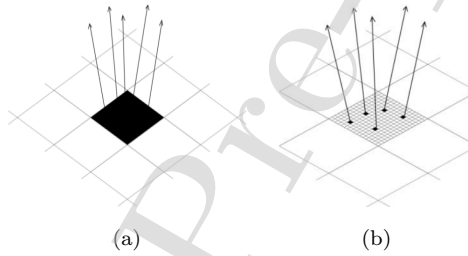


Figure 1: (a) Analogue and (b) Digital readout in the cell of a layer in the ECAL.

ECAL is affected by both the intrinsic shower fluctuations and the variations of the energy deposition per charged particle. The primary aim of a digital electromagnetic calorimeter (DECAL) is to suppress the last contribution by attempting to measure the number of charged particles directly. In Fig. 1, is shown an example of shower particles (drawn by arrows) passing through a cell of a sampling layer in the ECAL [2]. In Fig. 1 (a) silicon pads with analogue readout are used, measuring the energy deposited by the particles traversing, and in Fig. 1 (b) digital pixels are employed as shower particle counters. The feasibility to use Monolithic Active Pixel Sensors (MAPS) in the development of a highly granular DECAL with reasonable power consumption and cost has been proposed before [3, 4]. A recent attempt to assemble a composite calorimeter using MAPS is presented in Ref. [5].

## 2. Simulation results for digital readout

Simulations were conducted to evaluate the performance and the energy resolution of a DECAL within an ILC [6, 7] or a FCC detector [8]. A sampling calorimeter in octagonal barrel geometry, with 50 layers of MAPS with 18  $\mu\text{m}$  epitaxial Si as sensitive detector, was tested. The pixel pitch was  $50 \times 50 \mu\text{m}$  in counting pads of total area of  $5 \times 5 \text{ mm}^2$ . The absorber material was 2.1 mm thick tungsten and the performance was evaluated using single particle energy resolution [6]. As mentioned above, a digital calorimeter counts the numbers of particles in the shower which follows Poisson statistics. Then the uncertainty associated with the Landau fluctuations can be removed and the energy resolution approaches the intrinsic resolution. In Fig. 2 is shown the simulated energy resolution of the  $\sigma$  over the mean  $\mu$  of the number of particles. The mean particles per event shows a linear dependence up to 1000 GeV. The simulated

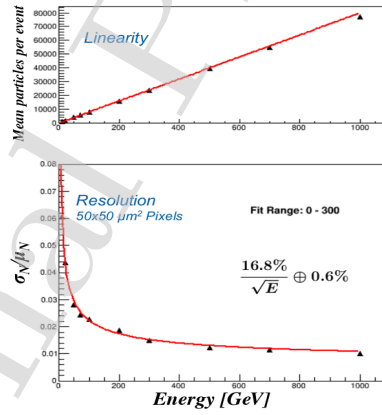


Figure 2: Top: Mean particles per event as a function of energy. Bottom:  $\sigma_N/\mu_N$  as a function of energy.

energy resolution extracted from a fit range from 0 to 300 GeV is  $16.8\%/\sqrt{E} \oplus 0.6\%$ . Above 300 GeV the particle density gets so high, that multiple particles are traversing a single pixel in a readout cycle, and the calorimeter performance gets non-linear.

### 3. The DECAL sensor

The DECAL sensor is a Monolithic Active Pixel Sensor, designed and fabricated in the TowerJazz 180 nm CMOS imaging process on 18  $\mu\text{m}$  epitaxial Si. The sensor matrix consists of  $64 \times 64$  pixels with a pitch of  $55 \times 55 \mu\text{m}$ . The pixel design implements four collection diodes placed in the pixel corners [9]. It has the advantages of low capacitance, optimum crosstalk reduction and good expected signal to noise ratio. Fig. 3 presents the simulated increase of the de-

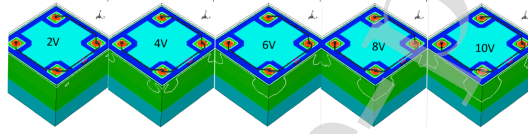


Figure 3: A simulated 3D pixel TCAD model of the DECAL sensor without the electronics on top of the pixel, under different bias voltages, using a simplified CMOS fabrication process [10].

pletion region below the diodes in the pixel, for bias voltages from 2-10 V. The CMOS imaging process provides the opportunity to add significant amount of electronics circuitry in the pixel [11]. For the current design of the DECAL sensor, each pixel contains a pre-amplifier, shaper, discriminator and the trimming logic of a 5 bit calibration DAC. The DAC itself is a binary weighted current mirror where the current is applied through a 31  $\text{k}\Omega$  resistor. This voltage is then sampled in either polarity by a capacitor in the path of the signal from the shaper, allowing the threshold to be tuned. With 5 bits, a granularity of the pixel trim up to 32 values is possible.

### 4. Data acquisition and analogue pixel test

For all the tests, the sensor is mounted on a custom designed PCB and read out with an Ethernet based readout system using the ATLAS ITSDAQ data acquisition software [12]. The PCB allows all the bias voltages and currents to be controlled by software. A hole cut into the PCB with a size of approximately  $4 \times 4 \text{ mm}^2$  allows access with a laser to the sensor substrate. As shown in Fig. 4 (a) the PCB is vertically mounted on the DECAL motherboard which

is connected to a Nexys Video board [13] through a FMC connector. The system allows a readout data rate of 40 MHz. The prototype pixel matrix has

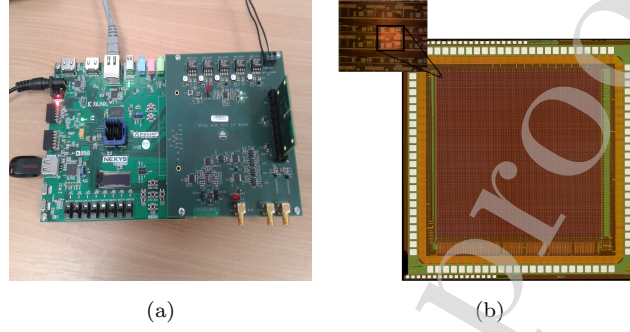


Figure 4: (a) Photograph of the DECAL boards used to hold the PCB with the mounted sensor and (b) Sensor layout with the analogue pixel in the top left corner.

one test pixel with analogue output, in the top left corner, as shown in Fig. 4 (b). From this analogue pixel, the pre-amplifier and shaper signals are read out with SMA connectors from the DECAL motherboard. The top left collection node from the analogue pixel is illuminated with a laser with a wavelength of 1064 nm and a maximum pulse frequency of 50 Hz. The laser beam focal spot size is  $10 \times 10 \mu\text{m}^2$ , the absolute laser intensity is calibrated and the injected charge is similar to that expected for a MIP. The calibration is done using a Si diode of 300  $\mu\text{m}$  thickness and an AMPTEK CoolFET A250CF charge sensitive amplifier. For low laser power conditions which correspond to a few tenths of pJ energy deposited per pulse, the injected charge was calculated to be 0.07 and 0.04 fC/ $\mu\text{m}$ , respectively. The above values correspond to 8000 and 4700e<sup>-</sup> equivalent injected charge in the 18  $\mu\text{m}$  epitaxial Si of the DECAL sensor. In Fig. 5 (a), are presented the measured pre-amplifier signals for 8000 and 4700e<sup>-</sup> injected charge compared to the simulated signals using 10 ns charge collection time. The simulated signals, consist of the pixel pre-amplifier output and the buffered signal by a source follower, which is loaded with a 1 k $\Omega$  resistor and a 5 pF capacitor. This is the signal that appears on the diode. Good agreement is observed in the rise time between the measured and simulated signals.

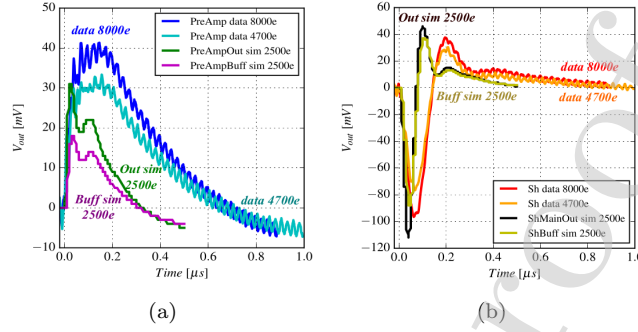


Figure 5: (a) Pre-amplifier and (b) Shaper signal for an injected charge of 8000 and 4700e<sup>-</sup> compared to the output and buffered signals of 2500e<sup>-</sup> input charge from Cadence simulations.

82 The injected charge during the tests is chosen to be two or three times higher  
 83 than the input charge in the simulation, as the laser beam is attenuated by the  
 84 metal and oxide layers before it illuminates the diode in the DECAL Si sensor.  
 85 This explains the residual difference in the amplitude between measured and  
 86 simulated signals. The longer decay times of the measured signals, is related  
 87 to the convolution of the diffusion collection time in the Si sensor with the pre-  
 88 amplifier response. The charge collection by diffusion is not included in the  
 89 Cadence simulations. In addition, Fig. 5 (b) shows the measured and simulated  
 90 shaper output and buffered signals for the same injected charge values. The  
 91 behaviour of the signal rise time, amplitude and decay time is similar to that  
 92 for the pre-amplifier signals.

## 93 5. Digital functionality and threshold scan results

94 The DECAL pixel matrix prototype is designed to be read out in two modes.  
 95 It can be reconfigured to function as either a strip sensor, for particle tracking, or  
 96 a pad sensor, counting the number of pixels above threshold for digital calorime-  
 97 try. In Fig. 6 (a) is presented the strip readout mode, which consists of 64 strips.  
 98 Each strip corresponds to a  $1 \times 64$  pixel column array and can record up to a  
 99 maximum of 3 hits per column. A channel speed of 320 Mbit/s is maintained for  
 100 each of the 16 output LVDS channels. The overall data rate is 320 Mbit/s  $\times$  16

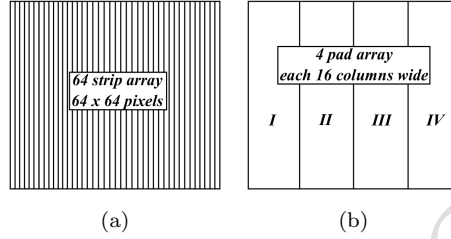


Figure 6: (a) Strip and (b) Pad readout mode.

thus 5.12 Gbit/s. The pad mode, Fig. 6 (b), consists of 4 blocks of strips. Each pad corresponds to a block of  $16 \times 64$  pixel column arrays and can record up to a maximum of 15 hits per column or a maximum of 240 ( $15 \times 16$  columns) total counts. The pad mode provides an overflow flag if the maximum number of counts is exceeded and can be operated at lower data rate. This is useful for digital calorimetry applications where the total number of hits is all that is required to measure the particle energy, but the data rate per area must be kept low as the total sensor area required is considerably larger than for tracking applications. The performance of the digital pixels is less straight-forward to evaluate than the analogue as there is no readout available for individual discriminator outputs. Performing a threshold scan in columns and rows using trimming logic, the rate of hits in each pixel allows to test the full chain from analogue to digital. In Fig. 7 (a) is presented a threshold scan under laser illumination, in strip mode with unmasked pixels and global chip configuration with all trim values set to zero. The laser IR light is emitted from a laser diode and a pulse frequency of 100 kHz. The laser was triggered using the clock from the daughterboard so that the readout could be synchronised with the laser pulse. With a defocused beam, hits recorded from around 10 strips, as the injected charge due to laser illumination on the individual pixels causes shaper output voltage drop. The plot shows a noise band at thresholds close to the shaper output rest level along with a clear signal response in the illuminated region with a shape reflecting the Gaussian profile of the laser. Using the laser trigger, the shaper response from a single strip is measured as a function of bunch

crossing time, Fig. 7 (b). The beam is focused to illuminate a single strip and

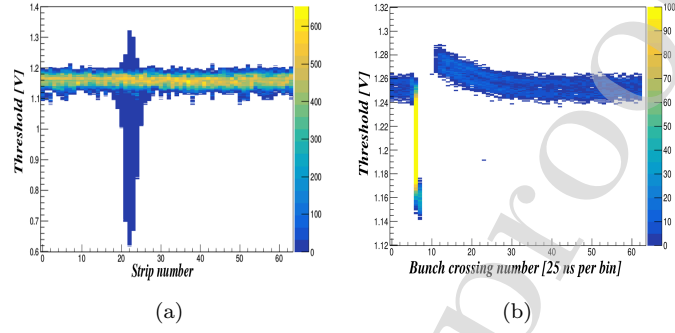


Figure 7: (a) Threshold voltage as a function of strip number and (b) Threshold voltage as a function of bunch crossing number.

124

125 the laser power is lowered. The time response is measured to be 25 ns. The  
 126 signal rise and decay time approximates the shaper output response measured  
 127 in the analogue pixel test, see section 4. Note that hits are only recorded when  
 128 the shaper output transitions from above to below the threshold. For the tests  
 129 shown in Fig. 8 the laser was switched off. Fig. 8 (a) shows the single pixel  
 noise,  $\approx 3$  mV, measured at the output of the shaper. In Fig. 8 (b) is shown the

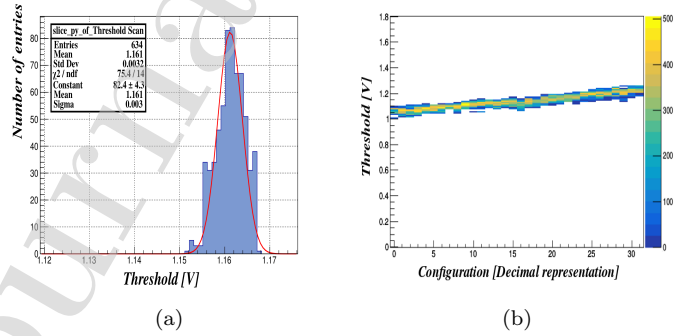


Figure 8: (a) Single pixel noise and (b) Threshold voltage as a function of pixel configuration.

130

131 measured single column response for all pixel configurations. The maximum 32  
 132 value in the x-axis, verifies the pixel threshold tuning from 5 bits. By changing  
 133 these 5 bits a smooth gradient is shown in the noise level with a maximum shift

134 of  $\approx 200$  mV. Combining this range with the noise level presented in Fig. 8 (a),  
 135 it is expected that in future the width of the noise band seen in Fig. 7 (a) could  
 136 be greatly reduced by applying trimming in every pixel. The final test of the  
 137 digital functionality is the comparison of the summing logic in strip and pad  
 138 mode under identical laser illumination conditions, presented in Fig. 9. With  
 139 a defocused laser beam 6 strips are fired at a global threshold value of 1 V, as  
 140 shown in Fig. 9 (a). Also the number of strips fired at 1 V, is verified from  
 Fig. 7 (a). The mean value of hits for each strip is approximately 3, which is

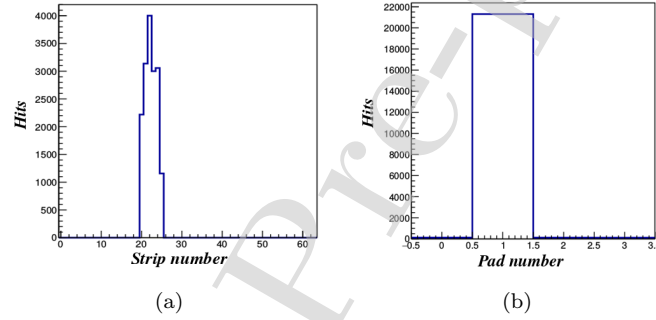


Figure 9: Hits in (a) strip and (b) pad mode at threshold voltage 1 V.

141  
 142 in agreement with the design specifications. Events with more than 3 hits are  
 143 recorded as 3, and the laser trigger repetition was chosen to be 1000. In Fig. 9  
 144 (b) is presented the pad mode operation for the same laser focus and power  
 145 conditions as in strip mode. As expected the 6 strips, number from 20 to 25,  
 146 fired in strip mode, corresponding to pad number 1. The sum of hits for the  
 147 6 strips is smaller than the total number of hits in pad number 1 since in pad  
 148 mode the maximum number of hits per strip can be up to 15. For each of the  
 149 4 pad channels, if the total counts 240 exceeded, an overflow flag appears and  
 150 is read out from a separate channel next to each pad channel. The difference in  
 151 the response shows the relative benefits and drawbacks of each mode. In strip  
 152 mode there is clearly more information on where each hit occurred due to the  
 153 higher granularity, however the integrated number of hits recorded is less than  
 154 that seen in pad mode. This is because the beam is defocused and it is hitting

more than 3 pixels per strip, so the strips are saturating and undercounting. For pad mode there is very little spatial information due to the large pad width. To verify that the difference in the integrated counts is due to the strips saturating, a further test is performed that measures the number of hits per laser pulse as a function of threshold. According to Fig. 7 (a), changing the threshold essentially changes the number of pixels that record a hit. The results of this test are presented in Fig. 10. An extra mode, binary strip, is included which

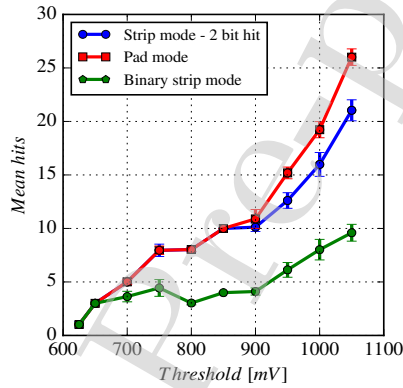


Figure 10: Mean value of hits as a function of threshold voltage for strip and pad operation mode.

corresponds to simply counting the number of strips with hit 1 or 0. At very low thresholds where one or two pixels are fired all three modes agree. For threshold above 700 mV, the binary mode saturates and starts to undercount as there are more than one hits per strip. The strip and pad mode agree up to  $\approx 10$  hits before the strip mode starts to undercount. At this threshold the beam area is greater than  $3 \times 3$  pixels and there are more than three hits per strip resulting in saturation. In strip mode with 2 bit hit information, a maximum of 3 hits per strip per laser pulse are recorded, so the mode is suitable for particle tracking due to limited summing logic. In pad mode, a higher number of hits per pad per laser pulse is recorded, this mode can be used for digital calorimetry. For binary strip mode, the mean value of hits corresponds to the number of strips fired for different threshold values, and the mode is suitable for particle tracking

with only available the strip address information. For strip and pad mode the quadratic increase of the mean value of hits as a function of threshold, is due to the high number of strips fired close to the threshold setting 1.1 V. In addition the Gaussian shape of the laser beam focus explains the small number of hits at low threshold where high laser power is required.

## 6. Conclusion

The reconfigurable DECAL sensor successfully demonstrates the digital functionality. The data read out according to design specifications in strip and pad mode, was verified with laser tests and pixel trimming. The capability of five bit pixel trim DAC improves substantially the pedestal and noise scans when the sensor is operating as a particle detector. The data acquisition system based on the ATLAS ITSDAQ, shows a reliable operation with perspective to be used in a future larger pixel matrix with higher data rate.

This work to develop a reconfigurable depleted MAPS sensor for digital calorimetry or tracking will continue with a new sensor, the RADECAL sensor. It will be designed and fabricated in the TowerJazz modified process [14] to improve the Si sensor radiation hardness performance. In addition, it will be modified to have the pixel trim range extended from five to six bits, where the sixth bit will be for pixel mask flag which de-activates the in-pixel comparator.

## 7. Acknowledgements

The authors gratefully acknowledge, the project funding received from the UK Research and Innovation - Science and Technology Facilities Council (STFC) Grant no. ST/N002911/1 and the project funding received from the European Union's Horizon 2020 Research and Innovation programme under Grant Agreement no. 654168.

## References

- [1] E. Garutti, *Overview on calorimetry*, Nucl. Inst. and Meth. A 628 (2011) 31-39, doi.org/10.1016/j.nima.2010.06.281.
- [2] M. Stanitzki et al., *A tera-pixel calorimeter for the ILC*, IEEE Nucl. Sci. Symp. Conf. Rec. (2007) 254–258, doi:10.1109/NSSMIC.2007.4436326.
- [3] The SPiDeR Collaboration, N. Watson et al., DESY PRC Report (2009), <http://www.hep.ph.imperial.ac.uk/calice/official/091105prc/spider.pdf>.
- [4] J.A. Ballin et al., *Design and performance of a CMOS study sensor for a binary readout electromagnetic calorimeter*, Journal of Instrumentation 6 (2011) P05009, doi.org/10.1088/1748-0221/6/05/P05009.
- [5] A.P. de Haas et al., *The FoCal prototype—an extremely fine-grained electromagnetic calorimeter using CMOS pixel sensors*, Journal of Instrumentation 13 (2018) P01014, doi.org/10.1088/1748-0221/13/01/P01014.
- [6] T. Price, *Digital calorimetry for future  $e^+e^-$  linear colliders and their impact on the precision measurement of the top higgs yukawa coupling*, PhD thesis, University of Birmingham, (2013).
- [7] A. Winter, *Prospects for higgs boson & top quark measurements and applications of digital calorimetry at future linear colliders*, PhD thesis, University of Birmingham, (2018).
- [8] T. Price, *Digital electromagnetic calorimetry at the FCC-hh*, Presentation at the third annual meeting of the Future Circular Collider Study, Berlin, 2017, <https://indico.cern.ch/event/556692/contributions/2465167>.
- [9] D. Das et al., *The OverMOS project*, Nucl. Inst. and Meth. A 824 (2016) 394-395, doi.org/10.1016/j.nima.2015.09.010.
- [10] E.G. Villani et al., *OVERMOS — CMOS Hi-Res MAPS detectors for HEP applications*, Nucl. Inst. and Meth. A 924 (2019) 78-81, doi.org/10.1016/j.nima.2018.08.033.

- 226 [11] R. Turchetta et al., *A monolithic active pixel sensor for charged particle*  
227 *tracking and imaging using standard VLSI CMOS technology*, Nucl. Inst.  
228 and Meth. A 458 (2001) 677-689, doi.org/10.1016/S0168-9002(00)00893-7.
- 229 [12] The ATLAS Collaboration, Technical Design Report for the ATLAS Inner  
230 Tracker Strip Detector, [https://cds.cern.ch/record/2257755/files/ATLAS-](https://cds.cern.ch/record/2257755/files/ATLAS-TDR-025.pdf)  
231 [TDR-025.pdf](https://cds.cern.ch/record/2257755/files/ATLAS-TDR-025.pdf).
- 232 [13] Nexys Video, [https://reference.digilentinc.com/reference/programmable-](https://reference.digilentinc.com/reference/programmable-logic/nexys-video/start)  
233 [logic/nexys-video/start](https://reference.digilentinc.com/reference/programmable-logic/nexys-video/start).
- 234 [14] W. Snoeys et al., *A process modification for CMOS monolithic ac-*  
235 *tive pixel sensors for enhanced depletion, timing performance and*  
236 *radiation tolerance*, Nucl. Inst. and Meth. A 871 (2017) 90-96,  
237 doi.org/10.1016/j.nima.2017.07.046.